

Experimental validation for low frequency isolation of six degree of freedom systems using inertial sensors

J Watchi¹, M.H.Lakkis^{1,2}, A.Sider², R.Jamshidi², A.Amorosi^{1,2}, M.Teloi¹, C. Collette^{1,2}

¹ Université Libre de Bruxelles, Beams, Precision Mechatronics Laboratory
Avenue F.D. Roosevelt 50, B-1050, Brussels, Belgium

² University of Liege, Aerospace Mechanical engineering, Precision Mechatronics Laboratory
Allée de la Découverte 9, 4000, Liege, Belgium

Abstract

After the first detection of gravitational waves in 2015 [1] a new era in understanding the universe took off. To make such detection, gravitational wave detectors are required to operate in an ultra stable environment that can be obtained only by isolating them from external disturbances. Active isolation control is a major approach in this context, it was successfully implemented in LIGO's positioning platform [2][3], where it is possible to obtain amplitude spectral densities lower than 10^{-12} m/ $\sqrt{\text{Hz}}$ for vertical and longitudinal seismic isolation at frequencies higher than 1 Hz. Nevertheless, it is still extremely challenging to obtain such good performances at lower frequencies. This paper addresses theoretical approaches and corresponding experimental validations for low frequency active damping and isolation of a six degree of freedom platform using super high resolution inertial sensors. The active platform is actively isolated by up to two orders of magnitude for frequencies between 0.1 Hz and 10 Hz.

1 Introduction

Precision control can be classified in two main categories [4], reference or point tracking and external disturbance rejection. External disturbance including sources such as seismic motion, human activity, and many other noise sources can play a significant role in limiting scientific setups requiring super high precision. Hence, comes the motivation to isolate some experimental setups from these external disturbances [5][6][7] using passive [8][9][10] and/or active approaches[11][12].

Such isolation is even more challenging at low frequencies where noise sources such as gravitational field fluctuation and seismic motion are more dominant. Moreover, the bigger the masses of bodies included in cosmological events the lower the frequency of gravitational waves caused by these events and hence the more challenging it is to detect them.

The concept of active inertial control is widely used in instrument isolation applications [13]. Furthermore, consider the one degree of freedom system in Figure 1 with a mass m and stiffness k .

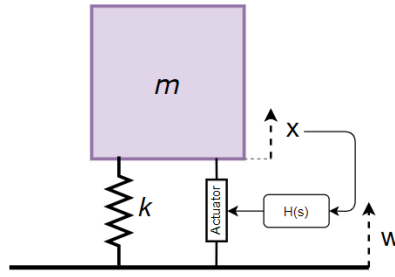


Figure 1: Sketch of a one degree of freedom system with inertial control on

By deriving the equations of motion, the compliance (transfer function from external disturbance force to mass displacement x) and transmissibility (transfer function from ground motion to mass displacement x) can be written respectively as:

$$T_{FX}(s) = \frac{X(s)}{F(s)} = \frac{1}{ms^2 + k} \quad (1)$$

$$T_{WX}(s) = \frac{X(s)}{W(s)} = \frac{k}{ms^2 + k} \quad (2)$$

The concept of active inertial isolation is based on feeding back the measured displacement of the mass into the actuators after passing it through a controller. Moreover, the equations of motion will yield to the following compliance and transmissibility curves when operating in closed loop:

$$T_{FX}(s) = \frac{X(s)}{F(s)} = \frac{1}{ms^2 + k + H(s)} \quad (3)$$

$$T_{WX}(s) = \frac{X(s)}{W(s)} = \frac{k}{ms^2 + k + H(s)} \quad (4)$$

Equations 3 and 4 show that as the controller gain tends to infinity, the transmissibility and compliance tend to zero too as the controller is in the denominator term. Hence, when applying high gains it is possible to isolate the displacement X of the mass from both, ground motion and external disturbance forces.

Figure 2 shows the transmissibility and compliance curves with and without inertial control. The controller used here is a simple gain with a derivative term, and it is capable to damp the resonance peak of the system (peak at 0.5 Hz is removed) and isolate the system (roughly speaking one order of magnitude from resonance frequency and below).

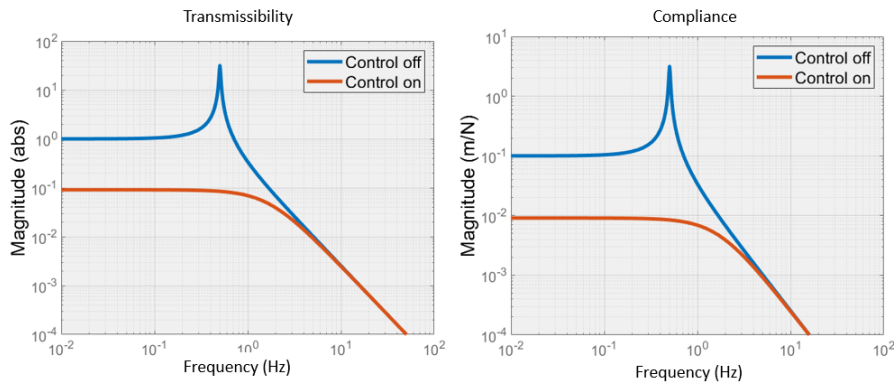


Figure 2: Transmissibility and compliance curves of a one degree of freedom system with control off and control on

2 Optical inertial sensors

Inertial sensors are one degree of freedom oscillating systems that return as an output the relative displacement between the sensor's base and the oscillating mass. Hence, assuming a simple inertial sensor that has a mass m , stiffness k and damping constant c as shown in figure 3, it is possible to write the sensitivity equation of these inertial sensors as follows:

$$T_{wy}(s) = \frac{Y(s)}{W(s)} = \frac{-ms^2}{ms^2 + cs + k} \quad (5)$$

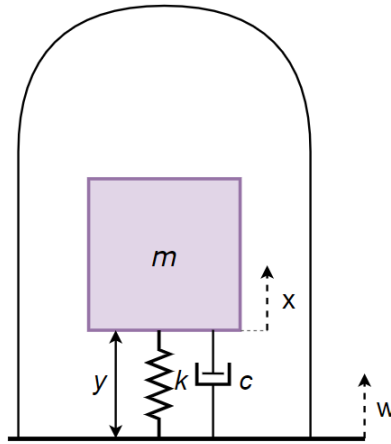


Figure 3: Sketch of the components of an inertial sensor

Equation 5 shows that for high frequencies (after resonance frequency of the system) the ratio of the relative displacement $Y(s)$ over $W(s)$ tends to one, this means that the relative displacement between ground and mass M gives a good measurement of the motion of ground W . However, for low frequencies (below the resonance frequency of the system), the ratio mentioned earlier is so small and converges to zero when going to lower frequencies, hence the sensor is not able to accurately measure ground motion.

Horizontal inertial sensors (HINS) and a vertical inertial sensors (VINS) that are used to actively isolate the platform were studied and developed by dr. Binlei Ding[14] and will be further discussed in next sections.

2.1 Horizontal inertial sensors

The working principle of the horizontal inertial sensor is very similar to what was introduced earlier, except that the one degree of freedom system under consideration is a pendulum (rotational equations of motion instead of translational). The information that could be read by the inertial sensor is also a relative displacement. More accurately by checking Figure 4 the readout of the sensor gives a measurement of $d - W_x$ with d being the absolute motion of the pendulum and W_x being the absolute motion of the platform where the sensor is placed in x direction.

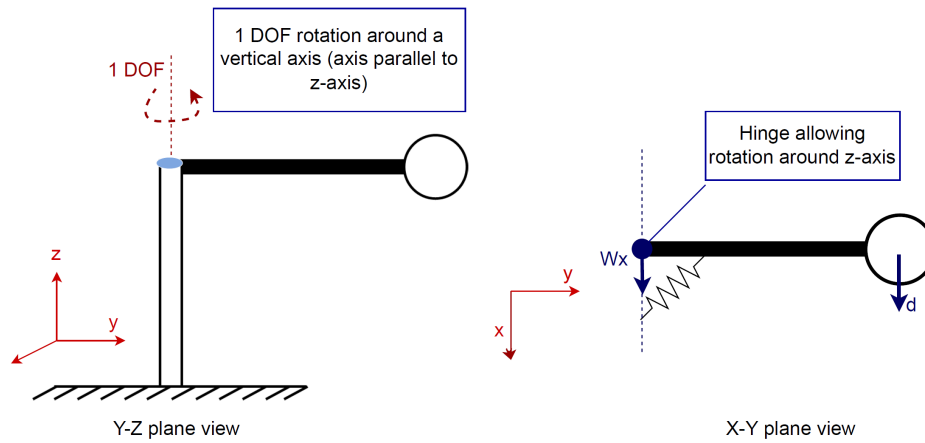
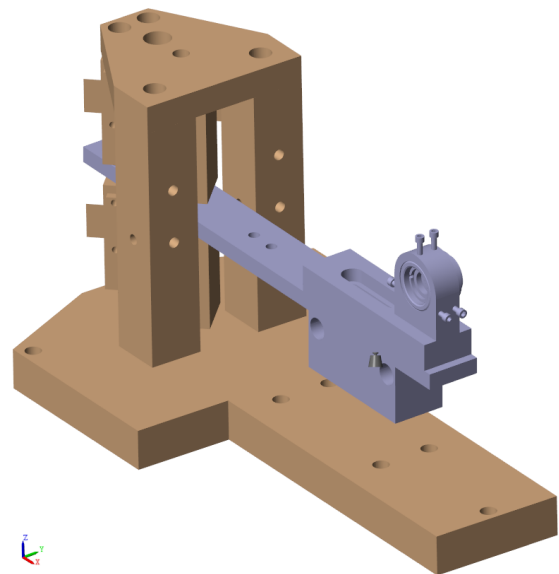


Figure 4: Sketch showing the working principle of Horizontal Inertial Sensor

Figure 5a shows the real inertial sensor and figure 5b shows a modeled version of the sensor (modeled using SimscapeTM[15]). It is modeled as a one degree of freedom oscillator where the stiffness, damping ratio and mass parameters are tuned in order to match the resonance frequencies of the model with the experimental peaks obtained when experimentally exciting the real plant.



(a) Real sensor



(b) SimscapeTM model of the sensor

Figure 5: Modeled and real horizontal inertial sensor used for the active isolation of the six degrees of freedom system

2.2 Vertical inertial sensors

The working principle of the Vertical inertial sensor is very similar to the principle of horizontal inertial sensor, as it is too a one degree of freedom, the only difference is that this pendulum operates in vertical direction as shown in Figure 6. Moreover, the information that could be read by the inertial sensor is also a relative displacement. More accurately by checking Figure 6 the readout of the sensor is $d - W_z$ with d being the absolute motion of the pendulum and W_x being the absolute motion of the platform where the sensor is placed along Z axis(vertical direction).

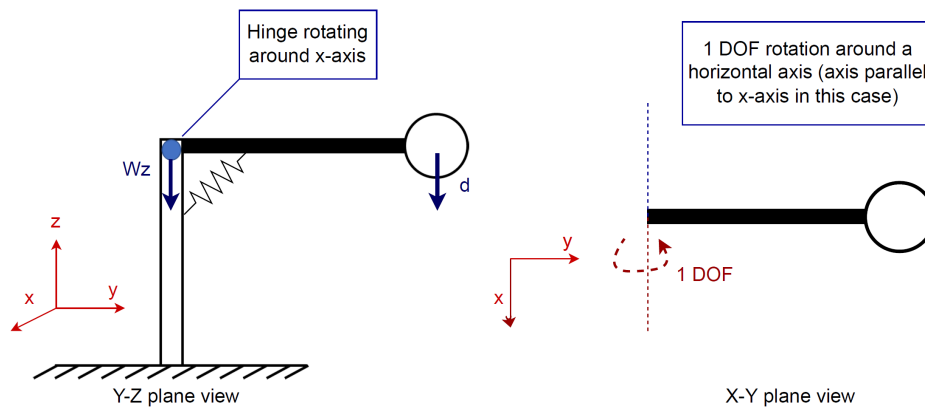
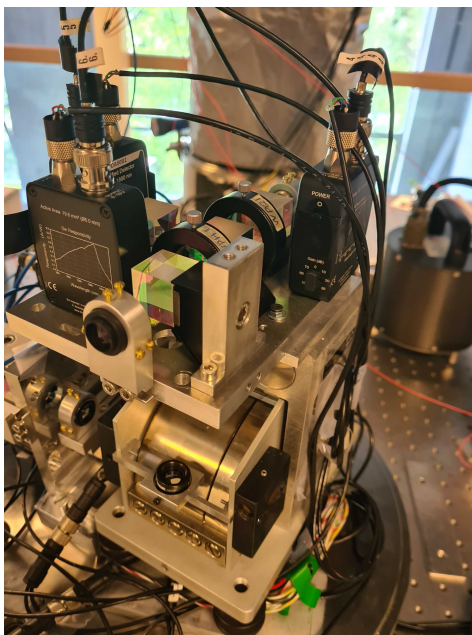
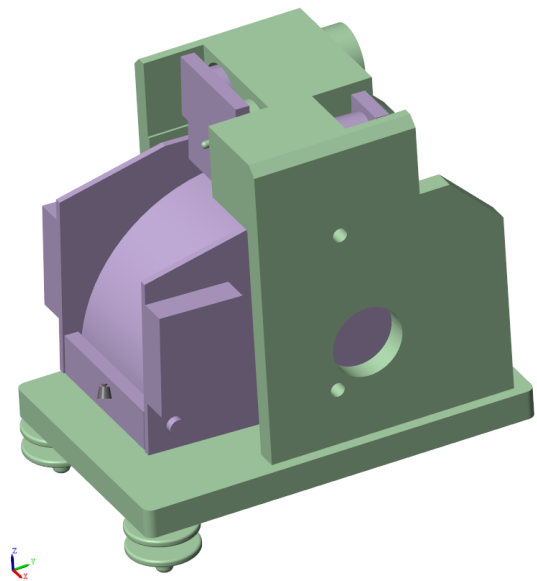


Figure 6: Sketch showing working principle of a vertical Inertial Sensor

Similar to the horizontal inertial sensor, the vertical one uses a Michelson interferometer [14] to readout the displacement of the proof mass with respect to the instrument frame, and it is also operated in vacuum at 0.1 mbar pressure. Figure 7a shows the real inertial sensor and Figure 7b shows a modeled version of the sensor [15]. It is modeled as a one degree of freedom oscillator where the stiffness, damping ratio and mass parameters are tuned in a similar manner as for horizontal inertial sensor.



(a) SimscapeTM model



(b) Real sensor

Figure 7: Modeled and real vertical inertial sensor used for the active isolation of the six degrees of freedom system

3 Active platform setup

The plant under study is a hexagonal shaped platform placed over six voice coil actuators and a passive stage. A SimscapeTM model for this platform was designed by dr. Jennifer Watchi [15] and can be shown in figure 8.

On the top of the active stage, three modules are added, each one of them constitutes of a vacuum chamber,

a horizontal inertial sensor and a vertical inertial sensor. The sensors are placed in a quasi collocated manner with the voice coil actuators that are modelled as force sources placed between the passive and active stage with actuation points on the bottom face of the hexagonal platform.

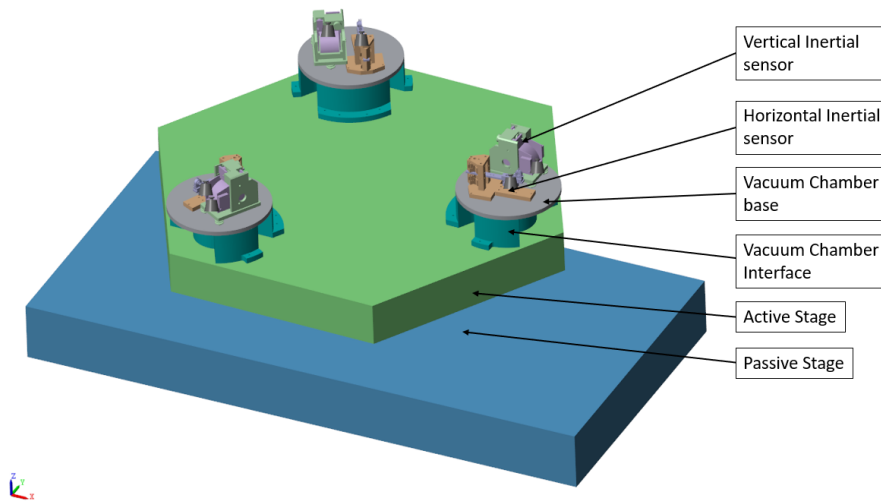


Figure 8: SimscapeTM model of the six degrees of freedom platform

Furthermore, the actuators and springs of the active stage are perfectly collocated. Actuators architecture can be shown in the sketch in Figure 9 where it is clear that every vertical actuator is perfectly collocated with a horizontal one and the three horizontal actuator-vertical actuator pairs are placed and oriented in a manner that corresponds to a third order rotational symmetry. Inertial sensors that are placed on top of the active platform are oriented in the same directions as the actuators.

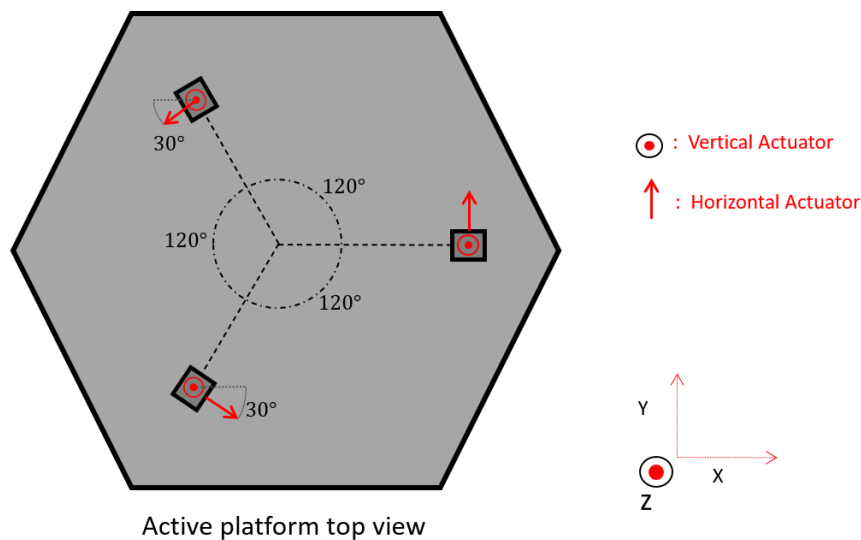


Figure 9: Sketch showing actuators positions and directions on the active platform

4 Active isolation control

It is worth to mention that the system has some sort of symmetry as there are three vertical sensors collocated with three vertical actuators, and three horizontal sensors collocated with three horizontal actuators. This

means that there will be two types of transfer functions in the diagonal elements of the transfer matrix (where each is repeated three times).

Moreover, the first and most basic control approach that could be followed is decentralised loop closing, where output signal from each sensor is feedbacked to its corresponding quasi collocated actuator.

Hence controllers will be designed according to diagonal elements of the open loop transfer matrix as they define relation between actuators and their corresponding collocated sensors:

4.1 Vertical open loop

Vertical open loop is the transfer function from a vertical actuator to its collocated vertical inertial sensor, such an open loop transfer function can be shown in Figure 10. The first peak at 0.24 Hz corresponds to the resonance frequency of the vertical inertial sensor, and other modes appearing between 1 Hz and 10 Hz correspond to the rigid body modes of the active platform.

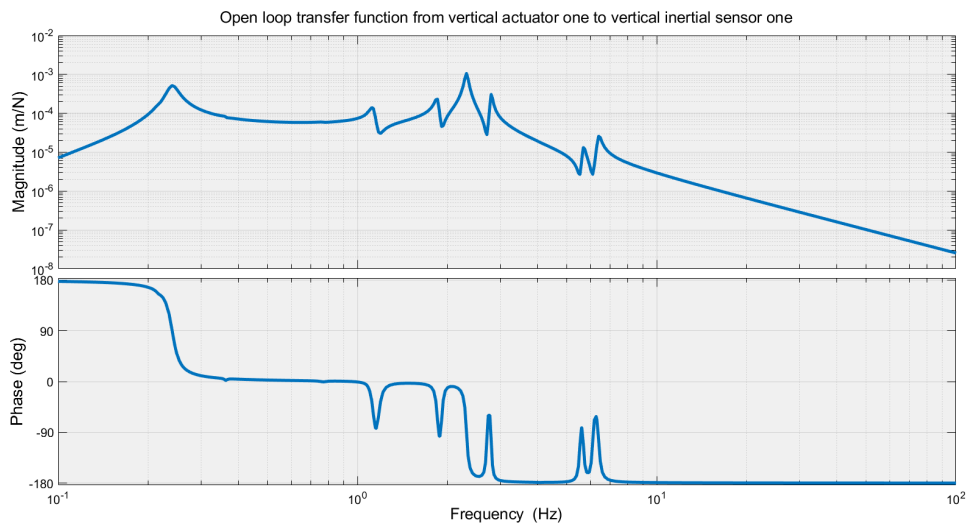


Figure 10: Open loop Transfer function from vertical actuator 1 to its collocated vertical inertial sensor

Moreover, in order to close the loop, a SISO approach will be considered when designing the controller. Hence, by checking the phase, it is converging to 180 degrees at low frequencies and -180 degrees at high frequencies. This justifies the need of a Lead-Lag controller in order to have better phase margins when introducing gains in the system. Moreover, the considered controller is shown in equation 6.

$$C_V(s) = 1.9739e11 \times \frac{(s)(s + 3.142)^2}{(s + 251.3)(s + 314.2)^2(s + 0.3142)(s + 0.06283)} \quad (6)$$

The *openloop* \times *controller* transfer function can be shown in Figure 11. When looking only on the transfer function and treating it as a SISO system, the controller introduced has a gain margin of 3.05 and a phase margin of 38.7 degrees.

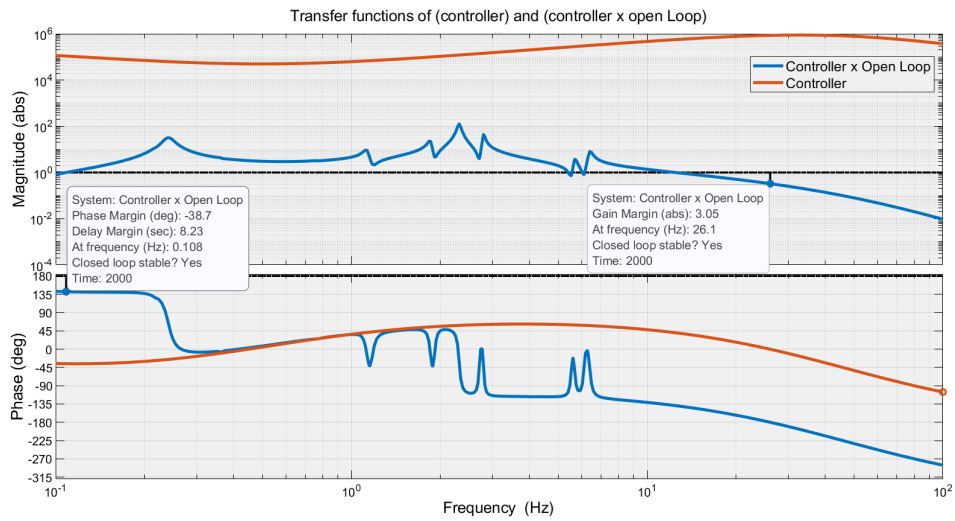


Figure 11: Open loop times controller transfer function from vertical actuator 1 to its collocated vertical inertial sensor

This controller constitutes of a lead with a zero at 0.5 Hz and a pole at 40 Hz, a lag with a zero at 0.5 Hz and the pole at 0.05 Hz, a second-order low pass filter with a corned frequency of 50 Hz, and a first-order high pass filter with a resonance frequency at 0.01 Hz. Moreover, this controller is used to feedback on the signals from the three vertical inertial sensors to their corresponding quasi-collocated actuators. The plant frequency response in a closed loop, shown in Figure 12, clearly indicates the control action in the frequency band 0.1-10Hz.

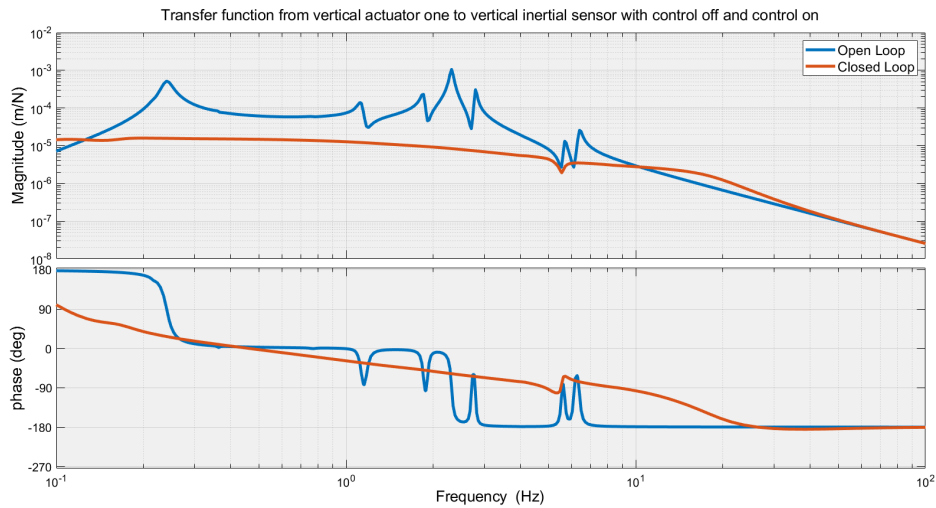


Figure 12: Open and close loop bode plots for transfer function from vertical actuator 1 to vertical sensor 1

4.2 Horizontal open loop

Horizontal open loop is the transfer function from a horizontal actuator to its collocated horizontal inertial sensor, such an open loop transfer function can be shown in Figure 13. By comparing open loop transfer function in horizontal direction when vertical directions are closed and when they are not, it can be shown that some peaks between 1 Hz and 10 Hz are removed because they correspond to rigid body modes that are controlled when closing vertical direction.

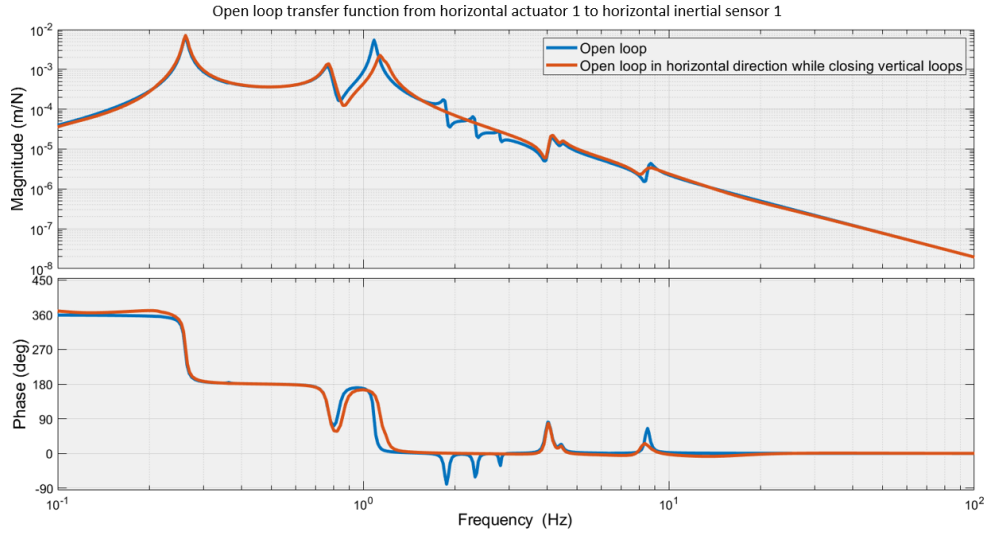


Figure 13: Open loop Transfer function from vertical actuator 1 to its collocated vertical inertial sensor

Moreover, to design the controller in horizontal direction the open loop plotted in orange in figure 13 should be considered. Similar to the case with vertical inertial sensors, the controller considered here is a lead-lag (Equation 7).

$$C_H(s) = -5.6998e09 \times \frac{(s)(s + 6.283)(s + 2.176)}{(s + 62.83)(s + 314.2)^2(s + 0.3142)(s + 0.06283)} \quad (7)$$

The *openloop* \times *controller* transfer function and stability margins can be shown in Figure14. However, since the considered system is a MIMO system, the notion of stability margins is not valid anymore as they do not indicate whether the whole MIMO system is stable or not, and if it is stable how far from instability it is. However, it is fair enough to say here that they help understand whether the system is pushed out of stability or not in the SISO loop being closed (but not in other loops).

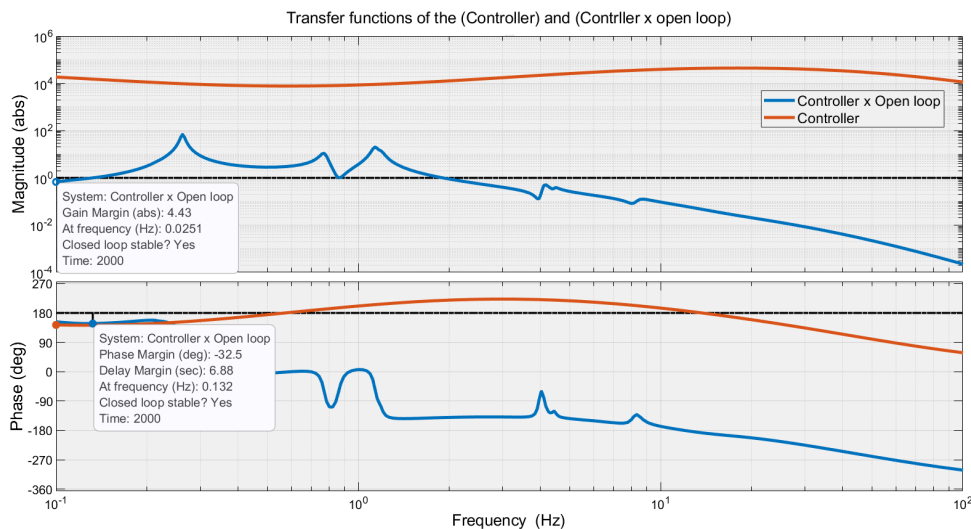


Figure 14: Open loop times controller transfer function from horizontal actuator 1 to its collocated vertical inertial sensor

To sum up, stability is not guaranteed by checking SISO phase and gain margin. So to ensure that it is on the stable side, the poles of the system were checked after closing all loops and they were all on the left half plane of the complex axis. The closed loop transfer function from first horizontal actuator to first horizontal

inertial sensor can be shown in Figure 15. It is clear that the control action is over a smaller bandwidth compared to vertical loop due to the fact that there is non minimum phase zero at low frequency which by it's role limits allowed gain in the system (this will be further discussed in section 4.4).

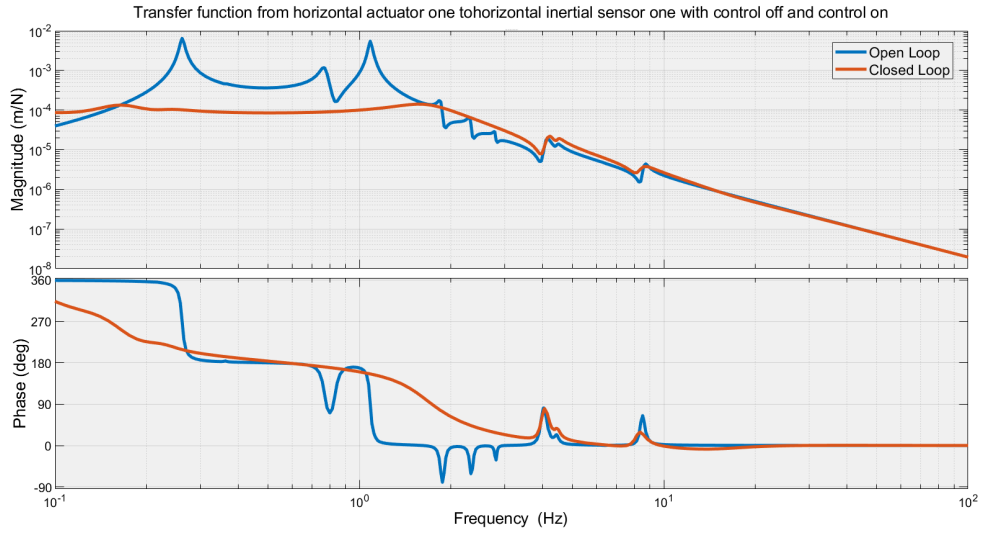


Figure 15: Open and close loop bode plots for transfer function from horizontal actuator 1 to horizontal sensor 1

4.3 Experimental validation

Everything described and implemented earlier was applied on the SimscapeTM model. However, since it is almost impossible to perfectly model the behaviour of the system, it is required to tune the controllers when implementing them on the real plant. Furthermore, the controllers were experimentally applied on the plant and the transmissibility was plotted using two seismometers (one placed on the active platform and the other on the ground). Experimental performance can be shown in Figure 16 for vertical direction and in Figure 17 for horizontal direction.

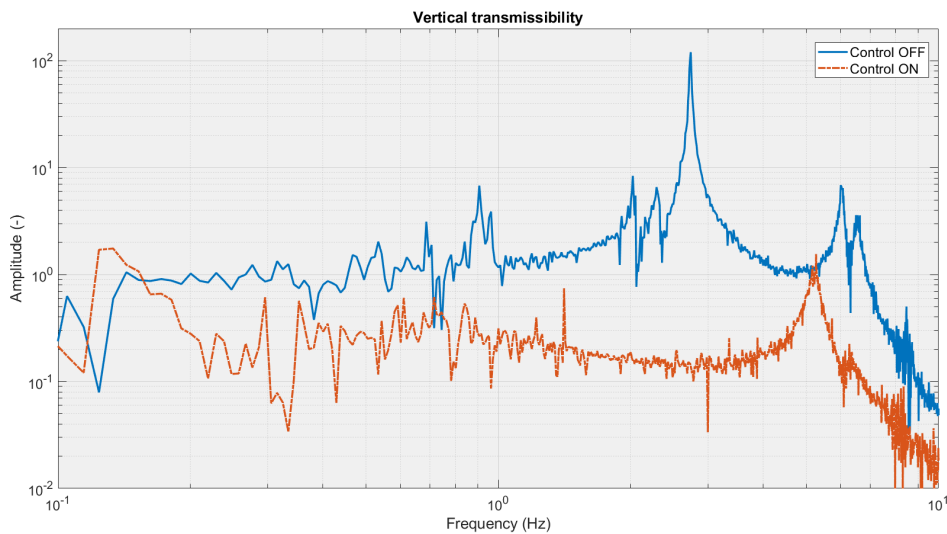


Figure 16: Experimental transmissibility measured from ground motion in vertical direction to active stage motion in vertical direction for control off and control on

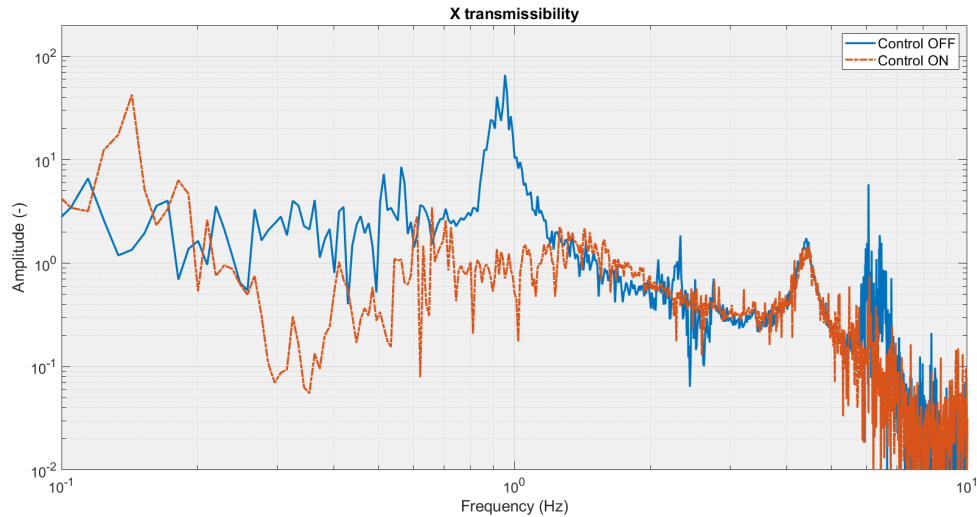


Figure 17: Experimental transmissibility measured from ground motion in X (horizontal) direction to active stage motion in X (horizontal) direction for control off and control on

Experimental results match what was expected from the model as the control bandwidth in vertical direction is clearly wider than that of horizontal direction. Isolation in vertical direction is around half order of magnitude between 0.1 Hz and 1 Hz and it averages around one order of magnitude between 1 Hz and 10 Hz. However, for horizontal direction the system is actively isolated by around a half order of magnitude between 0.2 Hz and 2 Hz. Moreover, the ASD plots of the displacements in the six degrees of freedom for control off and control on are added in the appendix.

4.4 Practical limitations

Practical limitations on the real plant can come from several sources, among them flexible modes, noise injected in the system, actuator-sensor configuration, etc... However, the first limitation faced experimentally here is non minimum phase zeros introduced in the system due to tilt-horizontal coupling. These zeros comes from the fact that the sensors are not able to differentiate between translation and tilting. Moreover, when applying very high gains, the poles of the closed loop system converge to the zeros of the open loop system, and since those zeros are non minimum phase (on the right half plane), the end result will be a closed loop system with right half plane poles and consequently an unstable system.

Since the SimscapeTM model includes the dynamics of the system, the no-minimum phase zeros are well modeled there. Moreover, several approaches with promising results were checked on the model to decrease the frequencies of those zeros, however, their practical implementation is still in progress. They are mostly based on (1) changing actuator-sensor configuration in such a way that it is possible to excite and sense translation and tilt in a more decoupled way and (2) controlling tilt in a more aggressive manner so that non minimum phase zeros are shifted to lower frequencies and more gains could be applied in the controllers at low frequencies. After that is implemented, it is expected to increase isolation up to two orders of magnitude for frequencies between 0.1 Hz and 10 Hz for both vertical and horizontal directions.

5 Conclusion

This paper goes in details of the process of controlling a six degree of freedom platform using six in vacuum optical inertial sensors and six actuators. Decentralised control approach was followed in closing six control loops on a Simscape model and then validated experimentally on the real plant. The platform was actively isolated in vertical direction between half and one order of magnitude for frequencies ranging between 0.1 Hz and 10 Hz. However, this isolation dropped down in horizontal direction where it was isolated by half

order of magnitude between 0.2 Hz and 2 Hz. Moreover, this is due to critical control limitations coming from non minimum phase zeros at low frequencies due to tilt horizontal coupling. Next steps are split in two main directions: (1) Decreasing the frequency of those non minimum phase zeros by modifying system architecture and calibrating sensors in such a way to actuate and sense in a more decoupled manner and (2) applying advanced control approaches such as MIMO decoupling, LQR, H-infinity and sensor fusion that could help push control performance further and decrease limitations coming from coupling.

Acknowledgements

The authors gratefully acknowledge the European Research Council, Consolidator grant SILENT (grant agreement number 866259) for funding this research. The authors also acknowledge the LIGO scientific community for reviewing this research. This paper has been assigned the LIGO DCC number P2200218.

References

- [1] B. Abbott, “Observation of gravitational waves from a binary black hole merger,” 02 2016.
- [2] F. Matichard, B. Abbott, S. Abbott, D. Coyne, and M. MacInnis, “Advanced ligo two-stage twelve-axis vibration isolation and positioning platform. part 1: Design and production overview,” *Precision Engineering*, vol. 40, 04 2015.
- [3] F. Matichard, B. Abbott, S. Abbott, and D. Coyne, “Advanced ligo two-stage twelve-axis vibration isolation and positioning platform. part 2: Experimental investigation and tests results,” *Precision Engineering*, vol. 40, 04 2015.
- [4] X. Li, J. Mcinroy, and J. Hamann, “Optimal fault tolerant control of flexure jointed hexapods for applications requiring less than six degrees of freedom,” vol. 4, 02 2000, pp. 3337 – 3338 vol.4.
- [5] M. Verma, V. Lafarga, M. Baron, and C. Collette, “Active stabilization of unmanned aerial vehicle imaging platform,” *Journal of Vibration and Control*, vol. 26, p. 107754632090549, 02 2020.
- [6] M. Verma and C. Collette, *Active Vibration Isolation System for Drone Cameras*, 01 2021, pp. 1067–1084.
- [7] T. Tang, S. Niu, T. Yang, B. Qi, and Q. Bao, “Vibration rejection of tip-tilt mirror using improved repetitive control,” *Mechanical Systems and Signal Processing*, vol. 116, pp. 432–442, 02 2019.
- [8] A. Stochino, B. Abbot, Y. Aso, M. Barton, A. Bertolini, V. Boschi, D. Coyne, R. Desalvo, C. Galli, Y. Huang, A. Ivanov, S. Marka, D. Ottaway, V. Sannibale, C. Vanni, H. Yamamoto, and S. Yoshida, “The seismic attenuation system (sas) for the advanced ligo gravitational wave interferometric detectors,” *Nuclear Instruments and Methods in Physics Research Section A: Accelerators, Spectrometers, Detectors and Associated Equipment*, vol. 598, pp. 737–753, 01 2009.
- [9] A. Wanner, G. Bergmann, A. Bertolini, T. Fricke, H. Lück, C. Mow-Lowry, K. Strain, S. Goßler, and K. Danzmann, “Seismic attenuation system for the aei 10 meter prototype,” *Classical and Quantum Gravity*, vol. 29, p. 245007, 11 2012.
- [10] Y. Akiyama, T. Akutsu, M. Ando, K. Arai, Y. Arai, S. Araki, A. Araya, N. Aritomi, H. Asada, Y. Aso, S. Bae, L. Baiotti, M. Barton, K. Cannon, E. Capocasa, C.-S. Chen, T.-W. Chiu, K. Cho, H.-Y. Chu, and Z.-H. Zhu, “Vibration isolation system with a compact damping system for power recycling mirrors of kagra,” *Classical and Quantum Gravity*, vol. 36, 05 2019.
- [11] L. Zuo and S. Nayfeh, “An integral sliding control for robust vibration isolation and its implementation,” *Proceedings of SPIE - The International Society for Optical Engineering*, vol. 5386, 07 2004.

- [12] R. Kirchhoff, C. Mow-Lowry, G. Bergmann, M. Hanke, P. Koch, S. Köhlenbeck, S. Leavey, J. Lehmann, P. Oppermann, J. Wöhler, D. Wu, H. Lück, and K. Strain, “Local active isolation of the aei-sas for the aei 10 m prototype facility,” *Classical and Quantum Gravity*, vol. 37, 06 2020.
- [13] G. Zhao, B. Ding, J. Watchi, A. Deraemaeker, and C. Collette, “Experimental study on active seismic isolation using interferometric inertial sensors,” *Mechanical Systems and Signal Processing*, vol. 145, p. 106959, 11 2020.
- [14] B. Ding, “Development of high resolution interferometric inertial sensors,” Ph.D. dissertation, Université libre de Bruxelles, Bruxelles, 2021.
- [15] W. Jennifer, “Active seismic isolation using interferometric inertial sensors,” Ph.D. dissertation, Université libre de Bruxelles, Bruxelles, 2022.

Appendix

A Nomenclature

ASD	Amplitude spectral density
DOF	Degree of freedom
$HINS$	Horizontal inertial sensor
$VINS$	Vertical inertial sensor
$T_{WX}(s)$	Transmissibility from ground motion to payload displacement
$T_{FX}(s)$	Transfer function from external force disturbance to payload displacement
$T_{wy}(s)$	Transmissibility from ground motion to sensor readout

B ASD Plots of Control off and Control on

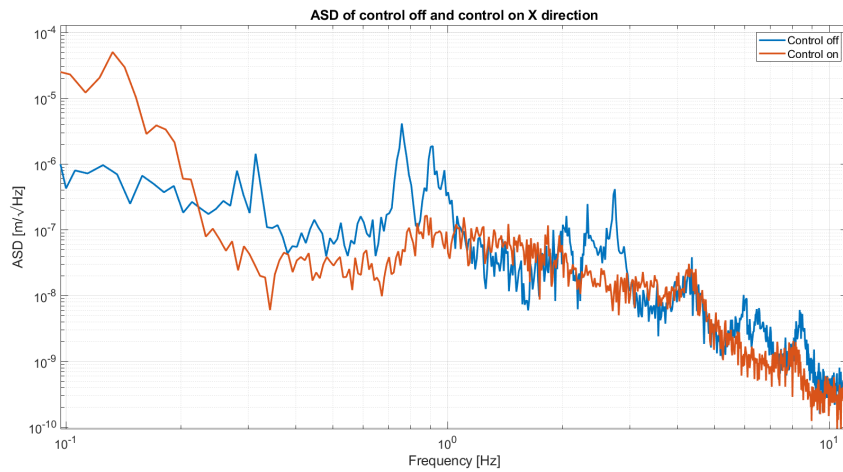


Figure 18: Displacement amplitude spectral density of the platform in X direction for control off and control on

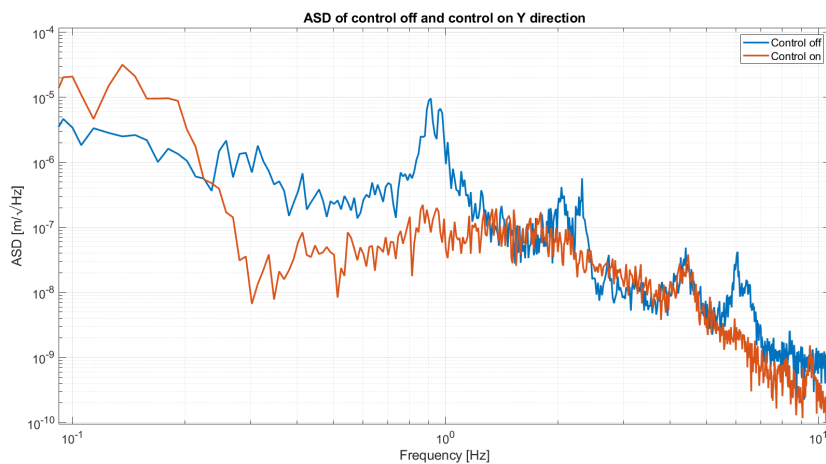


Figure 19: Displacement amplitude spectral density of the platform in Y direction for control off and control on

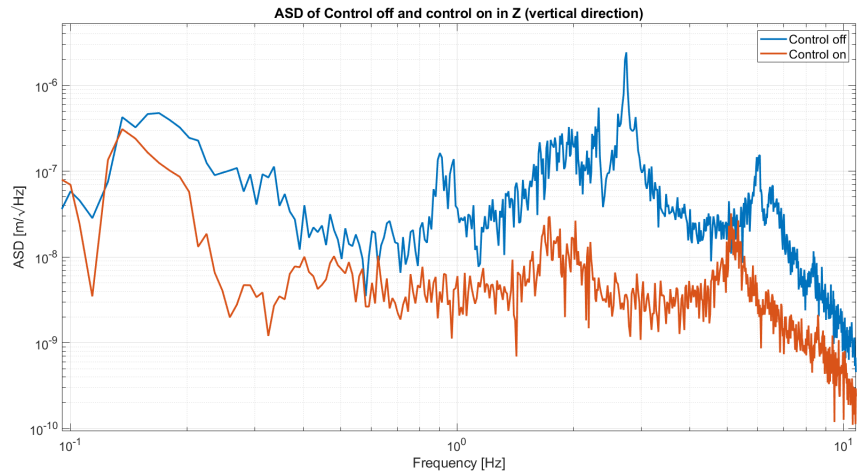


Figure 20: Displacement amplitude spectral density of the platform in vertical direction for control off and control on

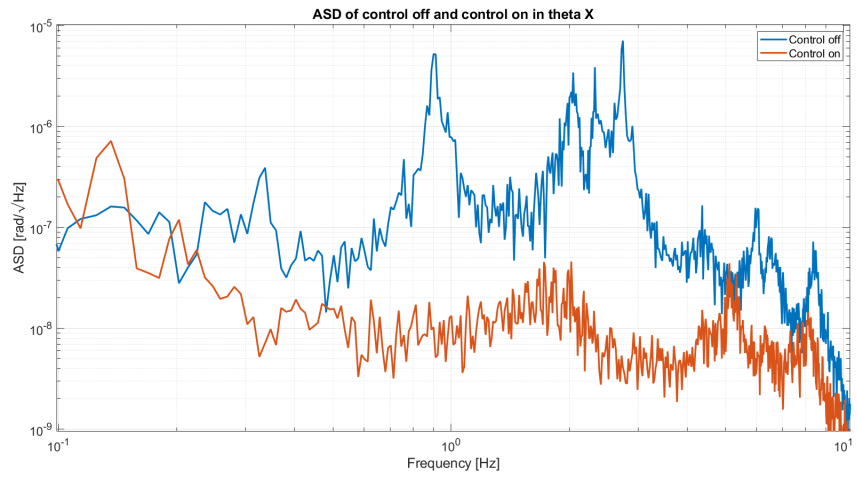


Figure 21: Angular displacement amplitude spectral density of the platform for rotation around X axis for control off and control on

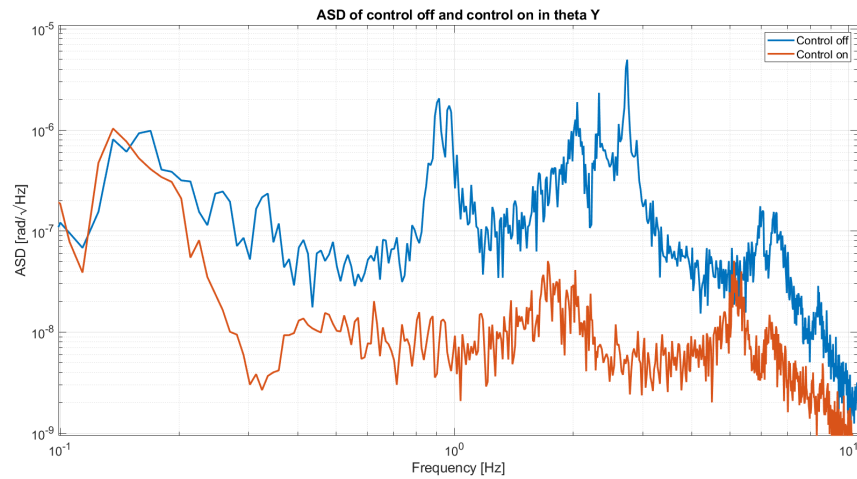


Figure 22: Angular displacement amplitude spectral density of the platform for rotation around Y axis for control off and control on

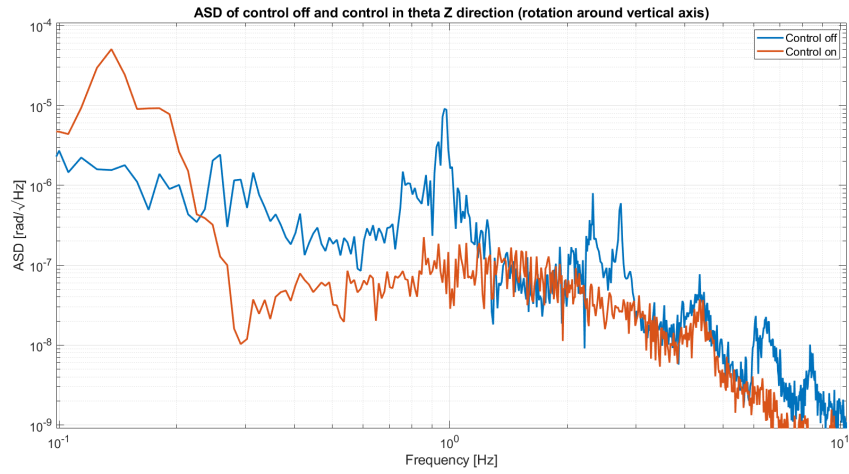


Figure 23: Angular displacement amplitude spectral density of the platform for rotation around Z axis for control off and control on